Critical Assessment of Two-Dimensional Methods for the Microstructural Characterization of Cemented Carbides

Shiqi Fang [1,2,*], Núria Salán [2], Christoph Pauly [3], Luis Llanes [2] and Frank Mücklich [3]

[1] Institute of Production Engineering, Saarland University, 66123 Saarbrücken, Germany
[2] CIEFMA-Department of Materials Science and Engineering, Universitat Politècnica de Catalunya, 08019 Barcelona, Spain
[3] Chair of Functional Materials, Saarland University, 66123 Saarbrücken, Germany
[*] Correspondence: shiqi.fang@uni-saarland.de

Abstract: Cemented carbides, or hard metals, are ceramic–metal composites usually consisting of tungsten carbide particles bound by a cobalt-based alloy. They are the backbone materials for the tooling industry, as a direct consequence of the outstanding range of property combinations, depending on their effective microstructural assemblage, i.e., the physical dimensions and relative content of their constitutive phases. Hence, reliable microstructural characterization becomes key for hard metal grade selection and quality control. This work aimed to assess the practical two-dimensional characterization methods for the most important one- and two-phase properties of cemented carbides, i.e., the carbide grain size, phase fraction, carbide contiguity, and binder mean free path. Three different methods—point, line, and area analysis—were implemented to characterize four microstructurally distinct grades. The images were acquired by optical and scanning electron microscopy, with the latter through both secondary and backscattered electrons. Results were critically discussed by comparing the obtained values of properties and the different characterization methodology. Inspection technique combinations were finally ranked based on accuracy, accessibility, and operability considerations. The line method was used to analyze all the properties, the area method, for the one-phase properties, and the point method, for only the phase fraction. It was found that the combination of optical microscopy and the line analysis method was suitable for a direct inspection and rapid estimation for carbides above fine grain size. The most precise results were achieved using line analysis of the images obtained by the backscattered electrons of the scanning electron microscope.

Keywords: cemented carbides; two-dimensional microstructural characterization; carbide grain size; phase fraction; carbide contiguity; binder mean free path; optical microscopy; SEM; EBSD

1. Introduction

Some of the most relevant mechanical properties of cemented carbides, such as hardness and toughness, may be quickly estimated from microstructural parameters, mainly carbide grain size and metallic binder content (phase fraction). In practice, carbide grain size is often offered by producers with a statistical estimation or qualitative classification such as: extra coarse, coarse, medium, fine, submicron, extra fine, etc. [1–6]. However, precise values of these properties are important for optimizing grade selection and quality control, and it becomes a practical need to find out quick, suitable, and reliable approximate characterization methods.

In research or industrial laboratories for production engineering, optical microscopes are usually the main choice for the direct inspection of tool materials. Common optical microscopes (OMs) include classic reflected light microscopes (metallographic microscope, digital microscope), white light interferometry, and confocal laser scanning microscopes [7,8]. In general, optical microscopes make use of visible light or lasers, and they

are capable of inspecting surface conditions on length scales as small as a micrometer. They can generally comply well with the physical dimensions of the constitutive phases of common tool materials. For example, cemented carbides basically have two-phase microstructures, and the carbide grain size varies from 6 μm to a submicron [9,10]. Normal optical microscopes are easy to operate without requiring special user training, and they usually do not demand specific environmental conditions. Therefore, they are suitable for the real-time inspection of the topographic or microstructural features of cemented carbides. However, the application of optical microscopes can be limited by their resolution, especially for grades containing a fine grain size (i.e., a mean size lower than 0.8 μm [1]). The borders of fine grains may become blurred due to insufficient sharpness or contrast, which leads to imprecise characterization regarding their geometric features.

The scanning electron microscope (SEM) is another common instrument used in research labs for material inspection, especially for acquiring information about surface topography. Moreover, the composition of materials can be observed with the aid of energy-dispersive X-ray spectroscopy. Instead of light, SEM uses electron beams to generate images of sample surfaces by capturing those particles after interacting with the sample surface or subsurface, such as secondary electrons (SEs) and backscattered electrons (BSEs) [11–16]. BSEs carry compositional information, as the backscattering power of the sample depends on its local atomic number. The resolution of SEM can reach levels as small as ~10 nm (BSE imaging) to ~1 nm (SE imaging), and it is theoretically suitable for the microstructural characterization of cemented carbides in the classes below fine grain size. However, SEM requires a large investment, and it is highly sensitive to ambient conditions. In addition, operators usually require special training. Hence, SEM is not as accessible as OM in labs.

In this study, the most representative one- and two-phase properties of cemented carbides, namely the carbide grain size, phase fraction, carbide contiguity, and binder mean free path, were targeted. The two aforementioned techniques, i.e., OM and SEM, were implemented to characterize four cemented carbide grades with different combinations of phase fraction and grain size. Three common two-dimensional characterization methods, namely point (PA), line (LA), and area analysis (AA) were proposed to analyze the images obtained by the two microscopy techniques. The referred microstructural parameters were determined using the free, open-source software, ImageJ [17,18]. This study aimed to assess these characterization methods by comparing the obtained properties to the nominal values offered by the manufacturer or obtained by more advanced techniques, such as electron backscatter diffraction (EBSD). Finally, these characterization methods, using various inspection techniques, were ranked based on their accuracy, accessibility, and operability considerations, in line with their practical applications.

2. State of the Art: Description of Analysis Methods

The following terms, i.e., carbide grain size, phase fraction, carbide contiguity, and binder free mean path, are often used to describe the microstructural assemblage of cemented carbides [19–22]. Carbide contiguity and binder free mean path are indeed two-phase parameters which can also be estimated from the single-phase ones, i.e., carbide grain size and phase fraction. Hence, all the obtained images were subject to the analysis of the phase fraction and grain size, using the three methods in this study: point (PA), line (LA), and area analysis (AA).

The amount of points (or lines) needed to be enough to effectively represent the feature dimensions with sufficient resolutions. According to the "Heyn Ruler Intercept Procedure"/"Heyn Method" (ASTM E112 or DIN EN ISO643), image dimensions should be determined in such a way that at least 50 grains are within the measuring range or the measuring lines should intersect a total of at least 50 grains. It was recommended in [23,24], to cut a minimum number of 200 grains in order to achieve the necessary statistical uncertainty (less than 10%). In this study, the grid sizes applied on different images were determined by time-consuming operations and result approximation, which depended on

the image size and nominal size of the geometric feature to be studied. The functions of the ImageJ software, "Analyze Grid and Multi-Point", were used to count the numbers. The theoretical considerations of these methods are given below.

2.1. Point Analysis (PA)

As shown in Figure 1a, in PA, a set of points was evenly deployed with identical intervals on the image. Hence, a homogenous grid of points covered the entire surface of the cemented carbide grades. Three different cases were then produced, complying with the localizations of the points:

- When the point was situated inside the grain, the point was counted as a valid point and then assigned the value of 1;
- When the point was situated outside the grain, it was counted as an invalid point and assigned the value of 0;
- In case the point was exactly at the grain boundary, it was counted as a half valid point, and assigned the value of 0.5.

Therefore, the valid number of the points N_c was the sum of the points inside the grains and at the grain borders. Assuming the total number of points was N_t, the phase fraction of grains f_g, or WC content was calculated by the equation:

$$f_g = \frac{N_c}{N_t}.$$

(1)

2.2. Line Analysis (LA)

As shown in Figure 1b, in LA, a set of horizontal and/or vertical lines was deployed with identical intervals on surface images. These lines intercepted both the WC particles and the metallic binder. Through these interceptions, the different parameters are defined as follows.

- WC grain size d_{WC}: It is the mean length of the linear intercepts within the WC phase. Its value was obtained by dividing the total intercept length Σl_{WC} by the WC grain number N_{WC}, as shown in the following equation:

$$d_{WC} = \frac{\Sigma l_{WC}}{N_{WC}}.$$

(2)

- Phase fraction of grains f_g: It is the equivalent to the ratio between the total intercept length within the grains Σl_{WC} and the total intercept length within the binder Σl_{Co}, as shown in the following equation:

$$f_g = \frac{\Sigma l_{WC}}{\Sigma (l_{WC} + l_{Co})}.$$

(3)

Contiguity C_{WC}: It is a two-phase parameter describing the carbide skeleton existing within the cemented carbide composites. It is defined as the fraction of the total number of grain–grain contact interfaces (WC–WC) and that of the grain–binder contact interfaces (WC–Co). It describes the coalescence behavior of grains in the metallic binder matrix, and such random distribution and orientation of grains is usually formed during the sintering process [25,26]. Precisely, $n_{\alpha\alpha}$ and $n_{\alpha\beta}$ are defined as the number of grains either touching or not touching each other, respectively, along the line. Contiguity is given with the following equation:

$$C_{WC} = \frac{2\,n_{\alpha\alpha}}{2\,n_{\alpha\alpha} + n_{\alpha\beta}}.$$

(4)

The parameter of contiguity had a value between 0 and 1. When the value of C_{WC} approached 1 (when $n_{\alpha\beta} = 0$), grain–binder contact decreased and grain–grain contact became more important. Meanwhile, when the value of C_{WC} approached 0 (when $n_{\alpha\alpha} = 0$),

grain–grain contact diminished. Contiguity decreased with increasing binder content or decreasing WC grain size. Contiguity is dependent on the processing conditions of cemented carbide.

- Mean free path (MFP) λ_{Co}: It is the other two-phase parameter and defines the mean length of the linear intercepts within the (cobalt) binder. It was calculated by dividing the total intercept length Σl_{Co} by the number of binder interceptions N_{Co}, as shown in the following equation:

$$\lambda_{Co} = \frac{\Sigma l_{Co}}{N_{Co}}. \tag{5}$$

The mean free path can be interpreted as the thickness of the binder. The MFP increased with rising grain size or binder content. When the MFP increased, fracture toughness increased and hardness decreased [27,28].

2.3. Area Analysis (AA)

As shown in Figure 1c, in AA, it was assumed that the total surface area was S_t, the grain area was S_g, and the phase fraction of grains (WC content) was f_g, calculated by the equation:

$$f_g = \frac{S_g}{S_t}. \tag{6}$$

The mean grain area A_g was obtained by dividing the grain area S_g by the number of grains N_g, and the equation is given as the following:

$$A_g = \frac{S_g}{N_g}. \tag{7}$$

For those "broken" grains situated on the image boundary, only half the number was counted.

Carbide grain size is related not only to the grain area but also to the grain shape. As the grain shape of cemented carbides is not uniformly determined in most cases, three shapes, i.e., circular, square, and equilateral triangle, are preliminarily defined and considered as the basic shapes of grains for estimation [6,29] Therefore, their size, i.e., circle diameter and lateral side length of the square or triangle, were obtained accordingly. The grain size d_g is defined as the equivalent to the mean value of their sizes, given as the following:

$$d_g = \frac{1}{3}\left(d_{g,circ} + d_{g,sq} + d_{g,tri}\right). \tag{8}$$

Where: $d_{g,circ} = 2\sqrt{\frac{A}{\pi}}$, $d_{g,sq} = \sqrt{2A}$, $d_{g,tri} = \sqrt{\sqrt{3}A}$

Although AA enabled the acquirement of the phase fraction and carbide grain size, two challenges still needed to be overcome during image processing: phase segmentation and grain determination. Precisely, grains needed to be separated from the binder and adjacent grains needed to be separated from each other. That way, the phase fraction and grain amount could be determined precisely. Common image processing software often offer tools or gadgets to realize such functions by detecting the color saturation or pixel contrast within images. For example, the tool "Analyze Particles" of the software ImageJ can measure the area by marking a color threshold and dividing the grains automatically. Meanwhile, the "Multi-Point" tool can count the grain amount and area. However, the accuracy of these tools is strongly dependent on the image quality, especially with respect to its contrast and resolution. Accordingly, more advanced microscopes or image processing software was necessary. For example, images obtained by SEM using a BSE detector usually offer a better contrast.
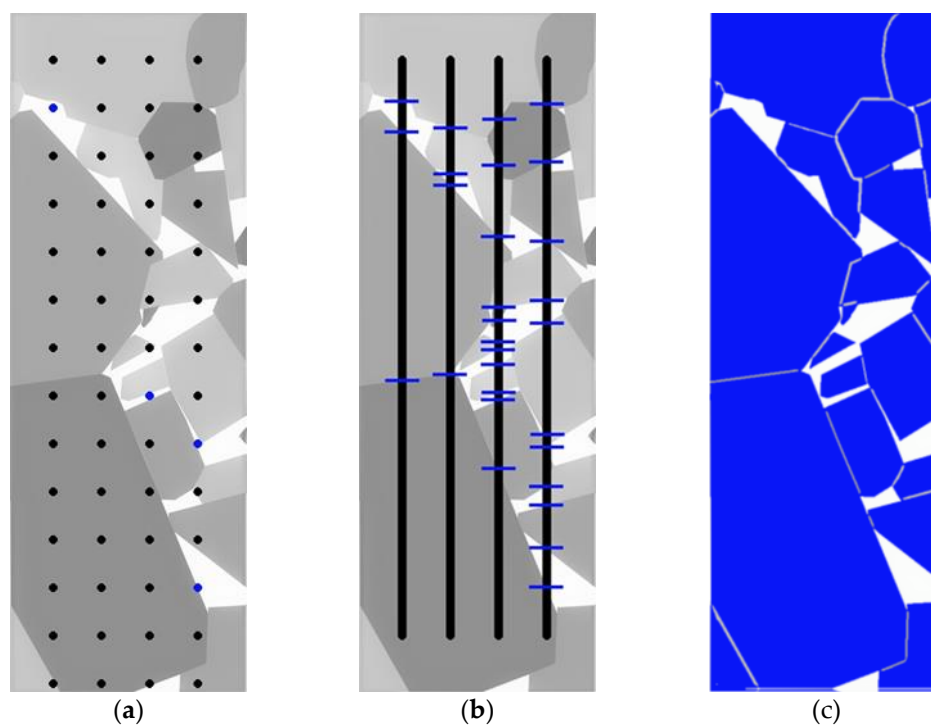
Figure 1. Schematic illustration of the analysis methods: (**a**) PA with black points situated inside the grains counted; (**b**) PA with blue strokes indicating the grain boundaries; and (**c**) AA with blue blocks indicating the grains.

3. Experimental Aspects: Materials and Sample Preparation

3.1. Sample Preparation

All the samples, with a dimension of 10 mm × 10 mm, were cold embedded in round silicon molds through exothermic polymerization (1:1 resin and hardener volume). They were then polished using the automatic polishing machine, ATM Saphir 520, following the program in Table 1. The Cameo disk, which consists of honeycomb patterns with embedded diamond particles, roughly removed the oxide layers on the HM samples under a water lubricating condition. Polishing disk MD-Allegro with honeycomb patterns was applied with the diamond suspension (DS 6 μm) to expose the microstructure of the HM samples. The polishing cloths, MD-Dac and MD-Nap, with corresponding diamond suspensions (DS 3 μm and DS 1 μm) were applied to finely polish the surface by eliminating tiny scratches or fine contaminations. In the final step, all the samples were cleaned with water and ethanol, and dried with compressed air before the inspection under microscopes. No etching was applied, as the carbide grain boundaries usually become very distinct to the binder after polishing.

Table 1. Sample preparation program.

Polishing Sequence	Cameo Disk	MD-Allegro	MD-Dac	MD-Nap
Lubricant	Water	DS 6 μm	DS 3 μm	DS 1 μm
Force (N)	20	20	20	20
Speed (rpm)	150	150	150	150
Time (min)	5	5	5	5

3.2. Studied Materials

3.2.1. Nominal Values of the One-Phase Properties of the Studied Hard Metal Grades

The samples studied refer to four hard metal grades with different combinations of binder content and carbide grain size, namely VN76, VN77, VGH2, and VG07. Their microstructural characteristics, as given by the supplier, are given in Table 2. Their density and hardness varied with their microstructure accordingly. The relative amount of WC in volume $vol.\%_{WC}$ was calculated by the following equation:

$$vol.\%_{WC} = \frac{\frac{wt.\%_{WC}}{\rho_{WC}}}{\frac{wt.\%_{WC}}{\rho_{WC}} + \frac{wt.\%_{Co}}{\rho_{Co}} + \frac{wt.\%_{Ni}}{\rho_{Ni}} + \frac{wt.\%_{Cr}}{\rho_{Cr}}}. \tag{9}$$

where the density information of the components are given as following: $\rho_{WC} = 15.63 \frac{g}{cm^3}, \rho_{Co} = 8.9 \frac{g}{cm^3}, \rho_{Ni} = 8.91 \frac{g}{cm^3}, \rho_{Cr} = 7.14 \frac{g}{cm^3}$.

Only the density of Co was considered for the calculation of the phase fractions in volume, as: (1) Ni and Cr largely dissolved in the Co phase, and were not present as pure elements; (2) Ni and Cr have similar densities; and (3) the amount of Cr was negligible.

Table 2. Microstructural characteristics of the cemented carbide grades studied.

HM Grade *	VN77	VN76	VG07	VGH2
WC (wt.%)	70%	70%	93%	89.7%
WC (vol.%) **	56.8%	56.8%	88.3%	83.0%
Ni (wt.%)	14.25%	14.25%	0%	0%
Co (wt.%)	14.25%	14.25%	7%	9.5%
Grain size (μm)	Extra coarse (>6.0)	Medium (1.3–2.5)	Extra coarse (>6.0)	Submicron (0.5–0.8)
Grain size (μm) ***	2.14	0.81	3.04	0.51
Density (g/cm³)	12.7	12.7	14.8	14.5
Hardness (HV30)	600	730	1180	1600

* VN77, VN76, and VGH2 may have contained a tiny amount of chrome (Cr). ** Phase fractions in volume were converted from those in weight. *** Grain size was obtained by electron backscatter diffraction (EBSD), referring to Table 3.

Information about the carbide grain size was given by the manufacturer with a descriptive classification; therefore, accurate grain size values became necessary for the assessment. In powder metallurgy, the term "grain" is often used to refer to individual powder particles, while in crystallography, "grain" is considered a synonym for "crystallite" with respect to the meaning of "boundary" in EBSD analysis. Therefore, a powder "grain", which consists of several crystallites, may have a larger size compared to the crystallite grain size obtained by EBSD. However, this is not the case for monocrystalline cemented carbide grains. Accordingly, the values of the grain size were measured by electron backscatter diffraction (EBSD). Although EBSD is time-consuming, it delivers the advantage of precisely extracting the data of crystal orientations, which allows for an exact separation of adjacent monocrystalline WC grains embedded in the binder matrix [30,31].

Integrated EBSD analysis software (EDAX OIM Analysis v7) can then generate grain size distributions and d_{WC} can be calculated using the following equation [32]:

$$d_{WC} = \frac{\Sigma d_i}{n}. \tag{10}$$

where d_i is the diameter of each individual grain, calculated from the grain area by the default approximation of circular shape.

Figure 2 shows an EBSD image of the grade VN77 as an inverse pole figure (IPF) map, as an example, and the four curves of the grain size distribution of the studied cemented carbide grades. The four curves basically met the classification of grain size. However, the obtained average values had slight deviations from the descriptive classification (Table 2). The obtained values of carbide grain size are listed in Table 3, and they serve as nominal data together with the data in Table 2 for the assessment. It is worth noting that the grain size estimated by EBSD may have been smaller than the actual one, since the analysis surface was randomly determined, and a two-dimensional slice could not cover the greatest stretch of all grains in a three-dimensional space. Moreover, the default approach of EBSD to grain size is to give the diameter of a circle of the same area which may also lead to deviations.
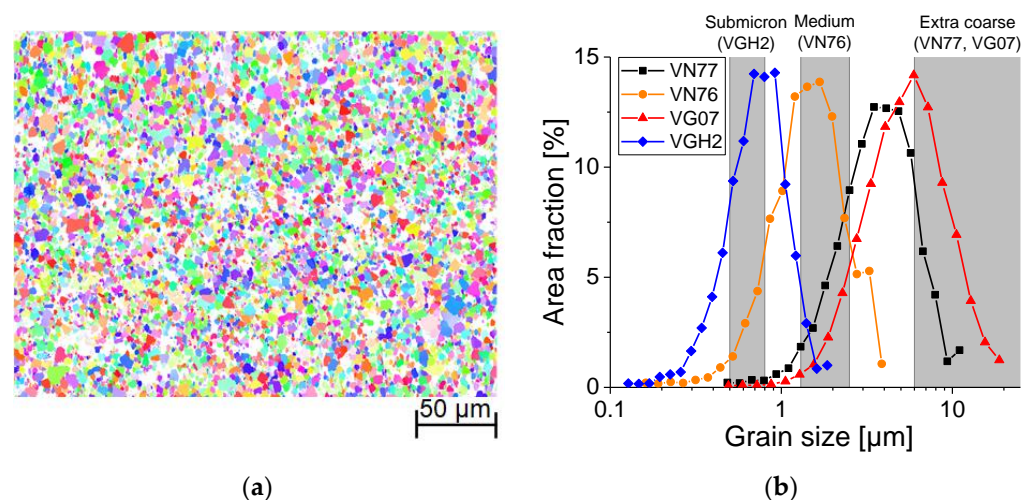

(**a**)

(**b**)

Figure 2. (**a**) An EBSD image of cemented carbide grades in inverse pole figure (IPF) representation, with VN77 as an example, and (**b**) the area fraction as a function of grain size of the four cemented carbide grades.

Table 3. Grain size in μm measured by EBSD with standard deviation.

HM Grade	VN77		VN76		VG07		VGH2	
Grain size/Deviation (μm)	d_{WC}	σ_{wc}	d_{WC}	σ_{wc}	d_{WC}	σ_{wc}	d_{WC}	σ_{wc}
Headings	2.14	1.44	0.81	0.58	3.04	2.11	0.51	0.26

3.2.2. Nominal Values of the Two-Phase Properties of the Studied Hard Metal Grades

Theoretically, it is not necessary to measure contiguity and mean free path as they can be derived from binder content and grain size using empirical equations [32,33]. Here, the following equations were used to calculate the two parameters:

$$\text{Contiguity: } C_{WC} = 1 - V_{Co}^{0.644} \, exp\left(\frac{0.391\sigma_{WC}}{d_{WC}}\right). \tag{11}$$

$$\text{MFP: } \lambda_{Co} = d_{wc}(1 - C_{WC})^{-1} V_{Co}(1 - V_{Co})^{-1}. \tag{12}$$

Knowing the nominal binder content V_{Co} (Table 2), grain size d_{WC}, and deviation σ_{WC} (Table 3), the nominal values of contiguity and MFP of each cemented carbide grade were calculated using the aforementioned equations (Table 4).

3.2.3. Reference Information of the Microstructural Parameters of the Studied Hard Metal Grades

The nominal values of all four properties were then summarized in Table 4, and used as a reference for the measured values.

Table 4. Nominal values of the four properties used as references for the assessment.

HM Grade	VN77	VN76	VG07	VGH2
Phase fraction/WC (vol.%)	56.8%	56.8%	88.3%	83.0%
Grain size (μm)	2.14	0.81	3.04	0.51
Contiguity C_{WC}	0.24	0.23	0.67	0.61
MFP λ_{CO} (μm)	2.15	0.80	1.22	0.27

3.3. Image Acquisition and Analysis Program

In this study, a confocal laser scanning microscope (LSM; Olympus Lext OLS3100) and a scanning electron microscope (SEM; FEI Helios Nanolab 600 and Thermo Fisher Helios G4 PFIB CXe, EDAX EBSD detector) were selected to acquire images of the microstructural features of the four cemented carbide grades under consideration. Together with the analysis methods, PA, LA, and AA, the values of the four properties were obtained with the program listed in Table 5.

Table 5. Details of the complete measurement program.*

Analysis Method	Image Acquisition **	Phase Fraction	Grain Size	Contiguity	MFP
	OM	✓	N.A.	N.A.	N.A.
PA	SE	✓	N.A.	N.A.	N.A.
	BSE	✓	N.A.	N.A.	N.A.
	OM	✓	✓	✓	✓
LA	SE	✓	✓	✓	✓
	BSE	✓	✓	✓	✓
	OM	✓	✓	N.A.	N.A.
AA	SE	✓	✓	N.A.	N.A.
	BSE	✓	✓	N.A.	N.A.

* ✓: applicable; ** OM: optical microscope, here, laser scanning microscope; SE: scanning electron microscope with secondary electrons; BSE: scanning electron microscope with backscattered electrons.

4. Results and Discussion

4.1. Image Acquisition

In general, optical microscopy is a quick process for estimations, while the SEM conducts more accurate characterization. However, the latter requires more time with limited access than the former. Examples of images and microscope configurations are shown in Figure 3 and Table 6. The SEM-BSE, which delivers a good phase contrast, achieved the best quality (resolution and clarity) for the microstructural characterization, followed by the SEM-SE and the OM. The OM was able to yield satisfactory surface images with enough contrast and clarity for the grade with coarse grain and high binder content, i.e., VN77. However, as grain size diminished to the medium level or the binder content decreased drastically, such as in the cases of VN76 or VG07, the OM images were reluctantly acceptable, as the contrast became quite limited due to restricted magnification capability. In the case of a fine carbide grain size and low binder content, such as in VGH2, the OM failed to obtain surface images with a satisfactory quality. Therefore, analysis based on the OM images of the grade VGH2 were omitted. The SEM was capable of obtaining SE images with good clarity of the four cemented carbide grades. However, the grain boundaries at some positions were blurry in the case of grades with a low binder content, such as in VGH2 and VG07. In contrast, the BSE delivered satisfactory images for all cases, as the boundaries could be well discerned with enough contrast and clarity between the grains and the binder.
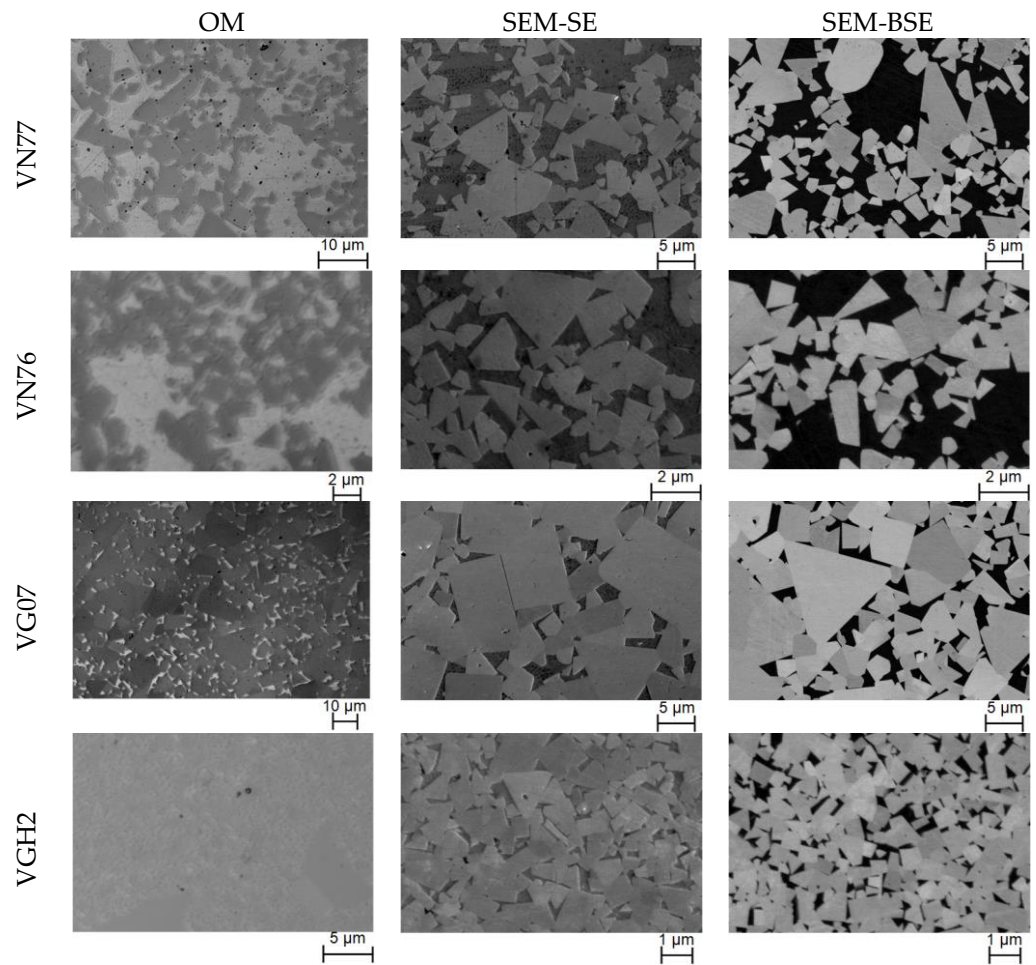
Figure 3. Microstructural images of the cemented carbide grades studied, obtained by: optical microscope (OM), i.e., laser scanning microscope in laser mode; scanning electron microscope with secondary electrons (SEM-SE); and SEM with backscattered electrons (SEM-BSE).

Table 6. Configurations of the implemented microscopes in Figure 3.

Image	Magnification	Objective Lens	Image	Magnification	Objective Lens
VN77 (OM)	2000	500 × 4	VG07 (OM)	4000	500 × 8
VN76 (OM)	4000	500 × 8	VGH2 (OM)	4000	500 × 8
Image	**Detector ***	**Acceleration Voltage**	**Horizontal Field Width (µm)**		
VN77 (SEM-SE)	ETD	5.00 KV	59.2		
VN76 (SEM-SE)	ETD	5.00 KV	25.9		
VG07 (SEM-SE)	ETD	5.00 KV	59.2		
VGH2 (SEM-SE)	ETD	5.00 KV	13.8		
VN77 (SEM-BSE)	CBS	5.00 KV	59.2		
VN76 (SEM-BSE)	CBS	5.00 KV	25.9		
VG07 (SEM-BSE)	CBS	5.00 KV	59.2		
VGH2 (SEM-BSE)	CBS	5.00 KV	13.8		

* ETD: Everhart–Thornley detector; CBS: concentric backscatter detector.

4.2. Microstructural Characterization

4.2.1. Point Analysis (PA)

The WC phase fractions were obtained by counting the points regularly located on the images. In total, three images obtained by each image acquisition approach were involved and an amount of about 50 points were counted in each case. The results are listed in Table 7 and compared in Figure 4. It was not possible to obtain a clear image of the grade, VGH2, by the OM due to resolution limitation. The measurement of phase fraction by PA turned out to be quite satisfactory in general, as the deviations from the nominal values of the PA (mean) in most cases were less than 4%. No obvious deviation differences in the results were observed among the three image acquisition methods or among the four studied grades.

Table 7. Phase fractions (vol%) of the WC grains obtained by the PA.

Phase Fraction	VN77		VN76		VG07		VGH2		Avg. Dev.
(vol%)	M	Δ	M	Δ	M	Δ	M	Δ	$|\overline{\Delta}|$
PA+OM	55.1%	−1.7%	64.3%	7.5%	90.8%	2.5%	-	-	3.9%
PA+SE	52.7%	−4.1%	59.8%	3.0%	93.8%	5.5%	85.7%	2.7%	3.8%
PA+BSE	53.7%	−3.1%	59.3%	2.5%	88.0%	−0.3%	85.2%	2.2%	2.0%
PA (mean)	53.8%	−3.0%	61.1%	4.3%	90.8%	2.5%	85.5%	2.5%	3.1%
N (nom. vol.%)	56.8%		56.8%		88.3%		83.0%		-

M: measured values; N: nominal values; $\Delta = M - N$; $\overline{|\Delta|} = (|\Delta|_{VN77} + |\Delta|_{VN76} + |\Delta|_{VG07} + |\Delta|_{VGH2})/4$.
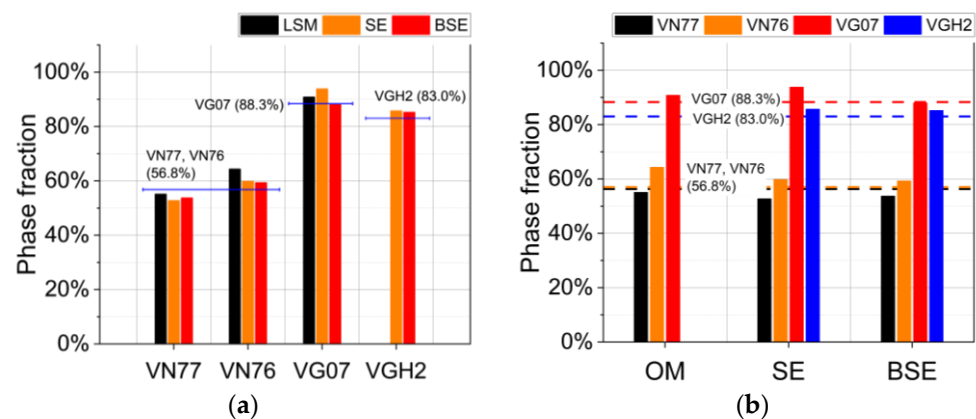

Figure 4. Results obtained by the point analysis (PA) of: (**a**) the phase fraction vs. cemented carbide grades, and (**b**) the phase fraction vs. image acquisition.

4.2.2. Line Analysis (LA)

The LA enabled a direct measurement of the most important one-phase microstructural parameters, i.e., phase fraction and carbide grain size, as well as the two two-phase parameters, contiguity, and mean free path (MFP). The measurements were carried out by regularly placing a set of 200 points on the obtained images and counting their identifications at these specific positions, i.e., grain–binder, binder–grain, and intergranular boundary. For each image acquisition method, three images were obtained and applied for the line analysis. Therefore, the LA turned out to be more time-consuming compared to the PA.

Phase Fraction

Measured values of phase fractions are listed in Table 8 and compared in Figure 5. The method exhibited satisfactory results, as the average deviations from the nominal values of the LA (mean) were less than 5%. However, the limitation of the LA+OM was proven to be more sensitive on the grades with a low binder content, i.e., VN76 and VGH2,

as the obtained deviation differences $\overline{|\Delta|}$ were much higher. Both methods, the LA+SE and the LA+BSE, achieved quite satisfactory results with deviations less than 3% for all cases.

Table 8. Phase fractions (vol%) of WC grains obtained by the LA.

Phase Fraction (vol%)	VN77		VN76		VG07		VGH2		Avg. Dev. $\overline{|\Delta|}$
	M	**Δ**	**M**	**Δ**	**M**	**Δ**	**M**	**Δ**	
LA+OM	64.7%	7.9%	68.9%	12.1%	87.9%	−0.4%	-	-	6.8%
LA+SE	55.6%	−1.2%	58.6%	1.8%	91.0%	2.7%	80.8%	−2.2%	2.0%
LA+BSE	58.9%	2.1%	57.9%	1.1%	85.6%	−2.7%	83.3%	0.3%	1.6%
LA (mean)	59.7%	2.9%	61.8%	5.0%	88.2%	−0.1%	82.1%	−0.9%	2.3%
N (nom. vol.%)	56.8%		56.8%		88.3%		83.0%		-

M: measured values; N: nominal values; $\Delta = M - N$; $\overline{|\Delta|} = (|\Delta|_{VN77} + |\Delta|_{VN76} + |\Delta|_{VG07} + |\Delta|_{VGH2})/4$.
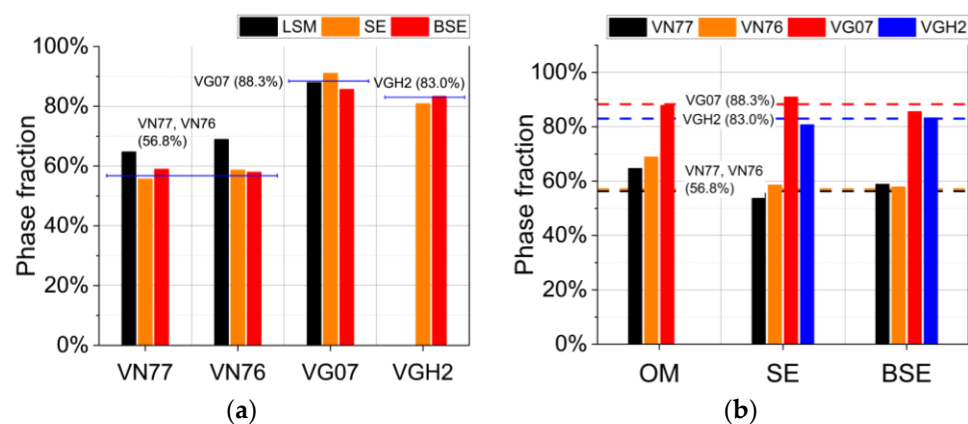

Figure 5. Results obtained by the line analysis (LA) of: (**a**) the phase fraction vs. cemented carbide grades, and (**b**) the phase fraction vs. image acquisition.

Grain Size

The measured values of carbide grain size are given in Table 9 and illustrated in Figure 6. The LA+BSE achieved the best results with an average deviation less than 8%. The LA+OM exhibited an obvious average deviation of 48.7%, and the deviation was more significant by the grade with a small grain size, VN76, as LA is strongly dependent on the determination of grain boundaries, which may be limited by LSM magnification and resolution. With respect to the LA+BSE, deviations were less pronounced by the cemented carbide grades with a small grain size (VN76 and VGH2).

Table 9. WC grain size by the LA.

Grain Size (μm)	VN77		VN76		VG07		VGH2		Avg. Dev. $\overline{|\Delta|}$
	M	**Δ**	**M**	**Δ**	**M**	**Δ**	**M**	**Δ**	
LA+OM	2.54	18.7%	1.45	79.0%	4.51	48.4%	-	-	48.7%
LA+SE	1.63	−23.8%	0.84	3.7%	3.56	17.1%	0.41	−19.6%	16.1%
LA+BSE	1.95	-8.9%	0.84	3.7%	2.65	−12.8%	0.48	−5.9%	7.8%
LA (mean)	2.04	−4.7%	1.04	28.4%	3.57	17.4%	0.45	−11.8%	15.6%
N (nom. EBSD)	2.14		0.81		3.04		0.51		-

M: measured values; N: nominal values; $\Delta = M - N$; $\overline{|\Delta|} = (|\Delta|_{VN77} + |\Delta|_{VN76} + |\Delta|_{VG07} + |\Delta|_{VGH2})/4$.
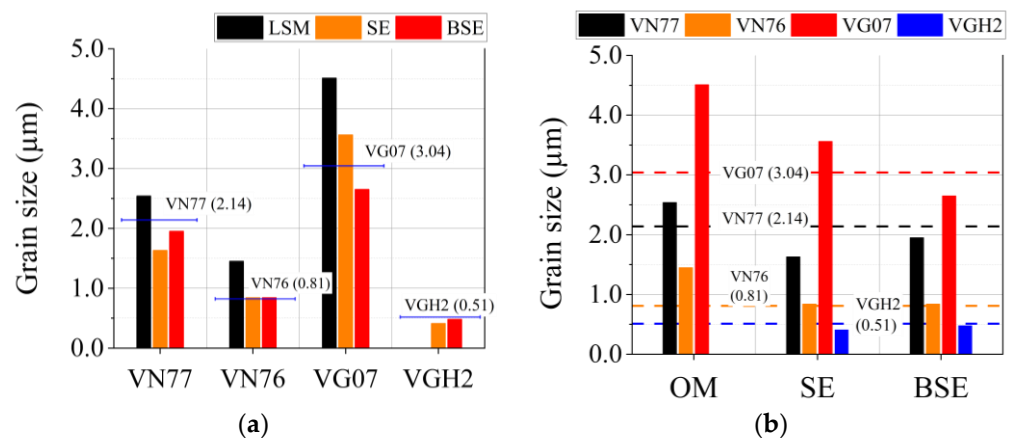
Figure 6. Results obtained by the line analysis (LA) of: (**a**) the grain size vs. cemented carbide grades, and (**b**) the grain size vs. image acquisition.

Contiguity and Mean Free Path (MFP)

The measured results of the two two-phase parameters are given in Tables 10 and 11, respectively. Contiguity is an index of the contacting grains. The nominal values mentioned are given in Table 3, and were obtained using empirical equations based on the phase fractions given by the producer. The grain sizes were obtained by EBSD measurement. Compared to the OM, the results obtained by the SEM images were closer to the nominal values, with only slight differences. The grades with a low binder content were proven to have obtained better approximation, as the results (LA (mean)) of the grades, VG07 and VGH2, were much closer to the nominal values (VG07: 0.71 vs. 0.67 and VGH2: 0.70 vs. 0.61) than those of the grades, VN77 and VN76 (VN77: 0.48 vs. 0.24 and VN76: 0.54 vs.0.23). Nevertheless, the empirical equations for the contiguity estimation did not consider the influence of the grain distribution, which might have led to more important deviations in the case of high binder grades [33]. Regarding the mean free path (MFP), the LA+BSE achieved the best approximation with the smallest average deviation value, followed by the LA+SE. Without considering the results obtained by the OM, the grades with a high binder content achieved a better approximation to the nominal values.

Table 10. Contiguity obtained by the LA.

Contiguity	VN77		VN76		VG07		VGH2		Avg. Dev.
	M	**Δ**	**M**	**Δ**	**M**	**Δ**	**M**	**Δ**	$\overline{\|\Delta\|}$
LA+OM	0.50	0.26	0.72	0.49	0.66	−0.01	-	-	0.25
LA+SE	0.58	0.34	0.41	0.18	0.74	0.07	0.66	0.05	0.16
LA+BSE	0.37	0.13	0.50	0.27	0.72	0.05	0.74	0.13	0.15
LA (mean)	0.48	0.24	0.54	0.31	0.71	0.04	0.70	0.09	0.17
N (nom. EBSD)	0.24		0.23		0.67		0.61		

M: measured values; N: nominal values; $\Delta = M - N$; $\overline{\|\Delta\|} = (\|\Delta\|_{VN77} + \|\Delta\|_{VN76} + \|\Delta\|_{VG07} + \|\Delta\|_{VGH2})/4$.

Table 11. Mean free path (MFP) obtained by the LA.

| MFP (μm) | VN77 | | VN76 | | VG07 | | VGH2 | | Avg. Dev. |
	M	Δ	M	Δ	M	Δ	M	Δ	|Δ|
LA+OM	2.17	0.02	1.58	0.78	0.97	−0.25	-	-	0.35
LA+SE	2.39	0.24	0.80	0.00	0.76	−0.46	0.18	−0.09	0.20
LA+BSE	1.95	−0.2	0.99	0.19	1.08	−0.14	0.24	−0.03	0.14
LA (mean)	2.17	0.02	1.12	0.32	0.94	−0.28	0.21	−0.06	0.17
N (nom. EBSD)	2.15		0.80		1.22		0.27		

M: measured values; N: nominal values; $\Delta = M - N$; $\overline{|\Delta|} = (|\Delta|_{VN77} + |\Delta|_{VN76} + |\Delta|_{VG07} + |\Delta|_{VGH2})/4$.

4.2.3. Area Analysis (AA)

Phase Fraction

The measured results of the phase fractions obtained by the area analysis are given in Table 12 and Figure 7. They matched well the nominal values, with an average deviation of less than 3%, except for those obtained by the OM. Similar to PA, no obvious difference was observed among the analysis methods or among the grades.

Table 12. Phase fractions (vol%) of WC grains obtained by the AA.

| Phase Fraction | VN77 | | VN76 | | VG07 | | VGH2 | | Avg. Dev. |
	M	Δ	M	Δ	M	Δ	M	Δ	|Δ|
AA+OM	44.1%	−12.7%	60.7%	3.9%	92.1%	3.8%	-	-	6.8%
AA+SE	56.0%	−0.8%	59.2%	2.4%	91.5%	3.2%	86.0%	3.0%	2.4%
AA+BSE	59.0%	2.2%	61.5%	4.7%	86.8%	−1.5%	84.4%	1.4%	2.5%
AA (mean)	53.0%	−3.8%	60.5%	3.7%	90.1%	1.8%	85.2%	2.2%	2.9%
N (nom. vol.%)	56.8%		56.8%		88.3%		83.0%		-

M: measured values; N: nominal values; $\Delta = M - N$; $\overline{|\Delta|} = (|\Delta|_{VN77} + |\Delta|_{VN76} + |\Delta|_{VG07} + |\Delta|_{VGH2})/4$.
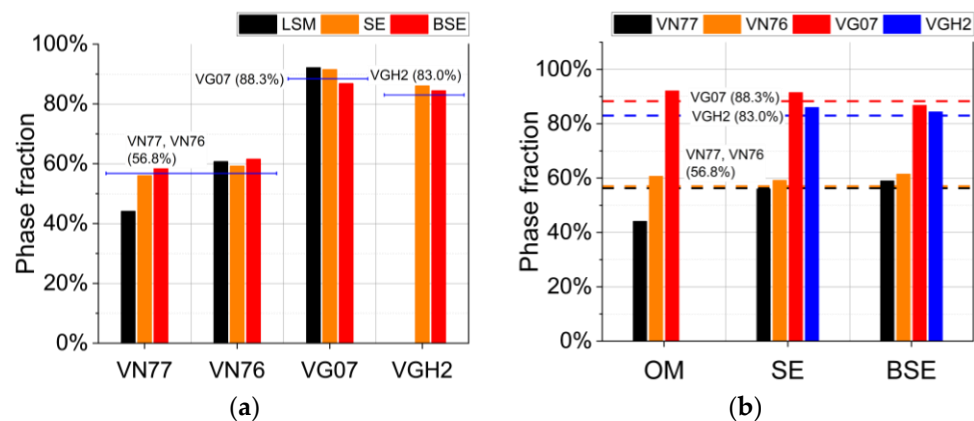
Figure 7. Results obtained by the area analysis (AA) of: (**a**) the phase fraction vs. cemented carbide grades, and (**b**) the phase fraction vs. image acquisition.

Carbide Grain Size

The results of the phase fractions obtained by the area analysis are given in Table 13 and Figure 8. The grain size was obtained based on the approximations of the three basic shapes, circle, square, and triangle, which appear most frequently in hard metals [6]. Similar to the LA, the AA+BSE achieved the best results with an average deviation around 25.1%, followed by the AA+SE, while the AA+OM exhibited a large gap with respect to the nominal values, with an average deviation around 85.4%. Unlike the LA, grain size or binder content did not exhibit much influence on the deviations, as the contacting grains

were separated using the "Automatic Function" of the software and estimated by the approximation of the three basic shapes. It is worth mentioning that the results of the AA+BSE and the AA+SE obtained by the approximation of the circle shape had only slight deviations between 10% and 15% compared to the nominal values, and the results matched well to the assumption of the circle shape during the nominal grain size measurement using the EBSD (Section 3.1).

Table 13. WC grain size obtained by the AA.

Grain Size (µm)	VN77		VN76		VG07		VGH2		Avg. Dev.
	M	Δ	M	Δ	M	Δ	M	Δ	$\overline{|\Delta|}$
AA+OM	3.06	43.0%	1.87	130.9%	5.54	82.2%	-	-	85.4%
Circle	2.68	25.2%	1.64	102.5%	4.86	59.9%	-	-	62.5%
Square	3.36	57.0%	2.06	154.3%	6.09	100.3%	-	-	103.9%
Triangle	3.13	46.3%	1.91	135.8%	5.66	86.2%	-	-	89.4%
AA+SE	2.25	5.1%	1.23	51.9%	4.09	34.5%	0.6	17.6%	27.3%
Circle	2.06	−3.7%	1.08	33.3%	3.59	18.1%	0.52	2.0%	14.3%
Square	2.28	6.5%	1.35	66.7%	4.49	47.7%	0.66	29.4%	37.6%
Triangle	2.4	12.1%	1.26	55.6%	4.18	37.5%	0.61	19.6%	31.2%
AA+BSE	2.41	12.6%	1.08	33.3%	3.98	30.9%	0.63	23.5%	25.1%
Circle	2.12	−0.9%	0.95	17.3%	3.49	14.8%	0.55	7.8%	10.2%
Square	2.65	23.8%	1.19	46.9%	4.37	43.8%	0.69	35.3%	37.4%
Triangle	2.47	15.4%	1.11	37.0%	4.07	33.9%	0.64	25.5%	28.0%
AA (mean)	2.57	20.1%	1.39	71.6%	4.53	49.0%	0.61	19.6%	40.1%
N (nom. EBSD)	2.14		0.81		3.04		0.51		-

M: measured values; N: nominal values; $\Delta = M - N$; $\overline{|\Delta|} = (|\Delta|_{VN77} + |\Delta|_{VN76} + |\Delta|_{VG07} + |\Delta|_{VGH2})/4$.
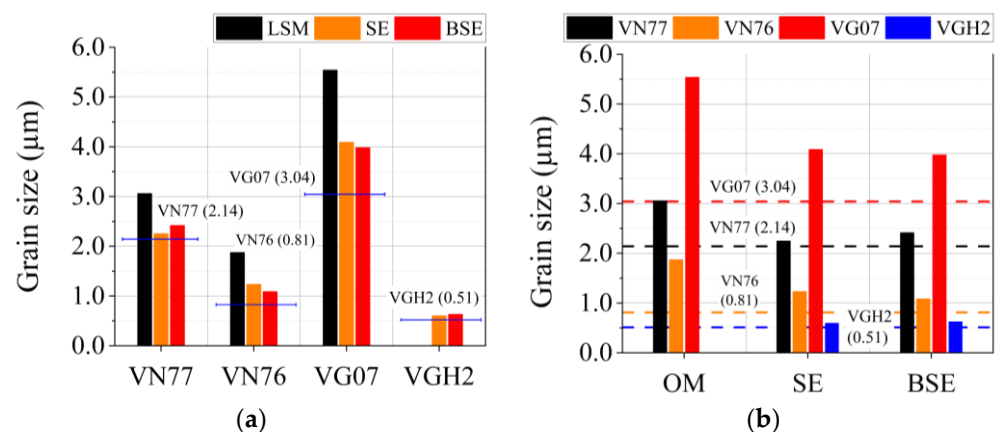

Figure 8. Results obtained by area analysis (AA) of: (**a**) the grain size vs. cemented carbide grades, and (**b**) the grain size vs. image acquisition.

4.3. Result Comparison of the Microstructural Characterization

According to the results in Section 4.2, the three analysis methods, in combination with the three different image acquisition methods, were systematically evaluated with three indices: accessibility, operability, and accuracy. Accessibility describes the possibility to access the equipment or software; operability reflects the operation difficulty and necessary time consumption; and accuracy represents the gap between the obtained values and the nominal ones. Four indicators qualitatively rated the evaluation indices: better than average (+), average (0), worse than average (−), and not applicable (N.A.). The evaluation is summarized in Table 14.

Table 14. Evaluation of the characterization and analysis methods for the one-phase properties.

Analysis Method	Image Acquisition *	Accessibility	Operability	Accuracy	
				Phase Fraction	Grain Size
PA	OM	+	+	+	N.A.
	SE	0	0	+	N.A.
	BSE	0	0	+	N.A.
LA	OM	+	0	0	−
	SE	0	−	+	0
	BSE	0	−	+	+
AA	OM	+	+	0	−
	SE	0	0	+	0
	BSE	0	0	+	0

* OM was not suitable for cemented carbides smaller than 0.8 μm, i.e., with a fine grain size.

In general, access to an optical microscope (OM) is much easier to obtain than to a scanning electron microscope (SEM), and a quick characterization and estimation of properties can be conducted using OM-obtained images. However, it should be noticed that the application of the OM may be limited by grain size and deviations may be caused to cement carbides with a grain size below microns [1]. Despite that the SEM achieved images with a better quality, it required much more time and preparatory work. Therefore, it may be recommended for precise characterization instead of quick estimation. The point analysis (PA) could only be applied for the measurement of the phase fraction, while the area analysis (AA) could measure both one-phase parameters. However, the AA might have led to some deviation when estimating grain size due to the approximation of grain shape. Compared to the PA and AA, the line analysis (LA) method was able to measure all the one- and two-phase parameters, i.e., the phase fraction, grain size, contiguity, and mean free path, although its conduction may have needed more time.

Regarding the phase fraction, all the methods achieved good or satisfactory results. However, when using the analysis methods combined with the OM, it was nearly impossible to characterize the cemented carbides with fine grain sizes due to the resolution and magnification limitations. Regarding the grain size, the LA and AA in combination with SE or BSE were able to conduct the measurement. The LA could achieve more satisfactory results despite its low operability compared to the AA.

To sum up the above, the OM may be recommended for a quick estimation of microstructural properties, including both phase fraction and grain size, as a result of its good accessibility and operability, and more precise results may be obtained by the BSE. Among the combinations of the image acquisition and analysis methods, the LA+BSE achieved the best approximation of grain size, as well as contiguity and mean free path [11–13]. However, attention should be paid to the influence of the binder, as a high content binder could lead to important deviations of contiguity approximations [25,33].

5. Concluding Remarks

In this study, four cemented carbide grades with a different binder content and grain size were characterized using different analysis methods, combined with surface images obtained by different microscopes. The obtained one- and two-phase microstructural properties, i.e., phase fraction, grain size, contiguity, and mean free path, were compared with nominal values. The comparison allowed for the assessment of the combinations of the different analysis methods and image acquisitions. Based on the assessment, the following recommendations may be made for the estimation of the properties of cemented carbides under different circumstances:

- In the case of rough estimation, the combination of line analysis and optical microscope (LA+OM) is a good and fast choice for the estimation of the one-phase properties of cemented carbides, and the two-phase properties may then be obtained using empirical equations.
- In the case of a more precise estimation, the combination of line analysis and backscattered electrons (LA+BSE) can be applied to measure all four properties of cemented carbides and yield precise results.

References

1. Schatt, W.; Wieters, K.-P.; Kieback, B. (Eds.) *Pulvermetallurgie*, 2nd ed.; Springer: Berlin, Heidelberg, Germany, 2007; pp. 504–540. https://doi.org/10.1007/978-3-540-68112-0.
2. Tarragó, J.M.; Coureaux, D.; Torres, Y.; Wu, F.; Al-Dawery, I.; Llanes, L. Implementation of an effective time-saving two-stage methodology for microstructural characterization of cemented carbides. *Int. J. Refract. Met. Hard Mater.* **2016**, *55*, 80–86. https://doi.org/10.1016/j.ijrmhm.2015.10.006.
3. Lay, S.; Missiaen, J.M. Microstructure and Morphology of Hardmetals. In *Comprehensive Hard Materials*; Elsevier: Amsterdam, The Netherlands, 2014; Volume 1, pp. 91–120, ISBN 9780080965284.
4. Jiménez-Piqué, E.; Turon-Vinas, M.; Chen, H.; Trifonov, T.; Fair, J.; Tarrés, E.; Llanes, L. Focused ion beam tomography of WC-Co cemented carbides. *Int. J. Refract. Met. Hard Mater.* **2017**, *67*, 9–17. https://doi.org/10.1016/j.ijrmhm.2017.04.007.
5. Fang, S.; Llanes, L. Microstructural characterization of cemented carbides by 3D volume reconstruction. *Mater. Charact.* **2020**, *159*, 110061. https://doi.org/10.1016/j.matchar.2019.110061.
6. García, J.; Ciprés, V.C.; Blomqvist, A.; Kaplan, B. Cemented carbide microstructures: A review. *Int. J. Refract. Met. Hard Mater.* **2019**, *80*, 40–68. https://doi.org/10.1016/j.ijrmhm.2018.12.004.
7. Davidovits, P.; Egger, M.D. Scanning laser microscope. *Nature* **1969**, *223*, 831–831. https://doi.org/10.1038/223831a0.
8. Bauer, W.; Weber, M.; Chanbai, S. White Light Interferometry. In *Encyclopedia of Tribology*; Springer: Boston, MA, USA, 2013; pp. 4115–4127. https://doi.org/10.1007/978-0-387-92897-5_320.
9. Engqvist, H.; Uhrenius, B. Determination of the average grain size of cemented carbides. *Int. J. Refract. Met. Hard Mater.* **2003**, *21*, 31–35. https://doi.org/10.1016/S0263-4368(03)00005-2.
10. Okamoto, S.; Nakazono, Y.; Otsuka, K.; Shimoitani, Y.; Takada, J. Mechanical properties of WC/Co cemented carbide with larger WC grain size. *Mater. Charact.* **2005**, *55*, 281–287. https://doi.org/10.1016/j.matchar.2005.06.001.
11. Seiler, H. Secondary electron emission in the scanning electron microscope. *J. Appl. Phys.* **1983**, *54*, R1–R18. https://doi.org/10.1063/1.332840.
12. Joy, D.C. Introduction to the scanning electron microscope. *Microsc. Microanal.* **2003**, *9*, 1556–1557. https://doi.org/10.1017/S1431927603447788.
13. Pérez-Arantegui, J. Electron microscopy. In *Reference Module in Chemistry, Molecular Sciences and Chemical*; Elsevier: Amsterdam, The Netherlands, 2017. https://doi.org/10.1016/B978-0-12-409547-2.14228-3.
14. Borgh, I.; Hedström, P.; Odqvist, J.; Borgenstam, A.; Ågren, J.; Gholinia, A.; Winiarski, B.; Withers, P.J.; Thompson, G.E.; Mingard, K.; et al. On the three-dimensional structure of WC grains in cemented carbides. *Acta Mater.* **2013**, *61*, 4726–4733. https://doi.org/10.1016/j.actamat.2013.05.008.
15. Mingard, K.P.; Roebuck, B.; Jones, H.G.; Stewart, M.; Cox, D.; Gee, M.G. Visualisation and measurement of hardmetal microstructures in 3D. *Int. J. Refract. Met. Hard Mater.* **2018**, *71*, 285–291. https://doi.org/10.1016/j.ijrmhm.2017.11.023.

16. Johansson, S.A.; Öhman, M.; Ekh, M.; Wahnström, G. CCBuilder: A software that produces synthetic microstructures of WC-Co cemented carbides. *Int. J. Refract. Met. Hard Mater.* **2019**, *78*, 210–218. https://doi.org/10.1016/j.ijrmhm.2018.09.011.

17. Rueden, C.T.; Schindelin, J.; Hiner, M.C.; DeZonia, B.E.; Walter, A.E.; Arena, E.T.; Eliceiri, K.W. ImageJ2: ImageJ for the next generation of scientific image data. *BMC Bioinform.* **2017**, *18*, 529. https://doi.org/10.1186/s12859-017-1934-z.

18. Schindelin, J.; Arganda-Carreras, I.; Frise, E.; Kaynig, V.; Longair, M.; Pietzsch, T.; Cardona, A. Fiji: An open-source platform for biological-image analysis. *Nat. Methods* **2012**, *9*, 676–682. https://doi.org/10.1038/nmeth.2019.

19. Roebuck, B.; Bennett, E.G. Phase size distribution in WC/Co hardmetal. *Metallography* **1986**, *19*, 27–47. https://doi.org/10.1016/0026-0800(86)90005-4.

20. Luyckx, S.; Love, A.D. Empirical quantitative relationships among grain size, mean free path, contiguity and cobalt content in WC-Co hardmetal. *Trans. R. Soc. S. Afr.* **2003**, *58*, 145–148. https://doi.org/10.1080/00359190309520469.

21. Brieseck, M.; Lengauer, W.; Gneiß, B.; Wagner, K.; Wagner, S. A straightforward method for analysing the grain-size distribution in tungsten carbide—Cobalt hardmetals. *Microchim. Acta.* **2010**, *168*, 309–316. https://doi.org/10.1007/s00604-010-0294-4.

22. *ISO 4499-2*; Hardmetals—Metallographic Determination of Microstructure—Part 2: Measurement of WC Grain Size. International Organization for Standardization: Geneva, Switzerland, 2018; p. 17.

23. Roebuck, B.; Bennett, E.G. *The Metallographic Measurement of Hardmetal Grain Size. Measurement Good Practice Guide No. 22*; National Physical Laboratory: Teddington, TW, USA, 2000. Available online: https://eprintspublications.npl.co.uk/1915/ (accessed on 1 July 2022).

24. Morrell, R.; Roebuck, B.; Bennett, E.G.; Lay, L.A. *Microstructural Measurement on Ceramics and Hardmetals. Measurement Good Practice Guide No. 21*; National Physical Laboratory: Teddington, TW, USA, 2007. Available online: https://www.npl.co.uk/gpgs/microstructural-measurements-on-ceramics-and-hardmetals (accessed on 1 July 2022).

25. Gurland, J. The measurement of grain contiguity in two-phase alloys. *Trans. Met. Soc. AIME* **1958**, *212*, 452–460.

26. Roebuck, B.; Mingard, K.P.; Jones, H.; Bennett, E.G. Aspects of the metrology of contiguity measurements in WC based hard materials. *Int. J. Refract. Met. Hard Mater.* **2017**, *62*, 161–169. https://doi.org/10.1016/j.ijrmhm.2016.05.011.

27. Lee, H.C.; Gurland, J. Hardness and deformation of cemented tungsten carbide. *Mater. Sci. Eng.* **1978**, *33*, 125–133. https://doi.org/10.1016/0025-5416(78)90163-5.

28. Pang, M.; Du, Y.; Zhang, W.; Peng, Y.; Zhou, P. A simplified hardness model for WC–Co–Cubic cemented carbides. *J. Min. Met. Sect. B Met.* **2021**, *57*, 253–259. https://doi.org/10.2298/JMMB200930021P.

29. Roebuck, B.; Phatak, C.; Birks-Agnew, I. *A Comparison of the Linear Intercept and Equivalent Circle Methods for Grain Size Measurement in WC/Co Hardmetals*; National Physical Laboratory: Teddington, TW, USA, 2004. Available online: https://eprintspublications.npl.co.uk/2947/ (accessed on 1 July 2022).

30. Mingard, K.; Roebuck, B. Interlaboratory Measurements of contiguity in WC-Co hardmetals. *Metals* **2019**, *9*, 328. https://doi.org/10.3390/met9030328.

31. Mingard, K.P.; Roebuck, B.; Bennett, E.G.; Gee, M.G.; Nordenstrom, H.; Sweetman, G.; Chan, P. Comparison of EBSD and conventional methods of grain size measurement of hardmetals. *Int. J. Refract. Met. Hard Mater.* **2009**, *27*, 213–223. https://doi.org/10.1016/j.ijrmhm.2008.06.009.

32. Wright, S.I. A parametric study of electron backscatter diffraction based grain size measurements. *Pract. Metallogr.* **2010**, *47*, 16–33. https://doi.org/10.3139/147.110060.

33. Golovchan, V.T.; Litoshenko, N.V. On the contiguity of carbide phase in WC-Co hardmetals. *Int. J. Refract. Met. Hard Mater.* **2003**, *21*, 241–244. https://doi.org/10.1016/S0263-4368(03)00047-7.